Pulsed ENDOR at 95 GHz on the Primary Acceptor Ubisemiquinone $Q_A^{-\bullet}$ in Photosynthetic Bacterial Reaction Centers and Related Model Systems

M. Rohrer,[†,‡,*] F. MacMillan,[§,△] T. F. Prisner,[†,‡] A. T. Gardiner,[§,¶] K. Möbius,[†] and W. Lubitz[§]

Institut für Experimentalphysik, Freie Universität Berlin, Arnimallee 14, D-14195 Berlin, Germany, and Max-Volmer-Institut für Biophysikalische Chemie und Biochemie, Technische Universität Berlin, Strasse des 17. Juni 135, D-10623 Berlin, Germany

Received: December 11, 1997; In Final Form: March 3, 1998

Davies-type pulsed ^{1}H electron nuclear double resonance (ENDOR) measurements were performed at a magnetic field of 3.4 T and a microwave (MW) frequency of 95 GHz (W-band). By taking advantage of the increased electron Zeeman interaction at high field, the small *g*-anisotropy of the semiquinone anion radicals could be resolved in frozen solutions. Hence, the W-band ENDOR spectra could be taken at the well-separated canonical peaks of the powder electron paramagnetic resonance (EPR) spectra, thereby becoming highly orientation-selective with respect to the relative orientation of the radicals to the external magnetic field. The measurements were performed on various randomly oriented semiquinone anion radicals in frozen alcoholic solution and on the primary ubiquinone anion radical, $Q_A^{-\bullet}$, in frozen photosynthetic bacterial reaction centers (RCs) of *Rhodobacter sphaeroides* in which the Fe was replaced by Zn (ZnRC). A simulation program was used to obtain magnitudes and orientations of the hyperfine tensors. The W-band ENDOR spectra of the immobilized radicals show not only hyperfine couplings (HFC) of local protons of the semiquinones, but also those of protons from the environment. These are, for example, involved in hydrogen bonds between the amino acid surrounding and the quinone carbonyl groups. For $Q_A^{-\bullet}$ in ZnRCs, a particularly large H-bond HFC was obtained from which direction and distance of the H-bond could be estimated. These data were compared with those measured for the respective ubisemiquinone radical, UQ-$10^{-\bullet}$, in protonated and deuterated 2-propanol, where two H-bonds of comparable strength but different directions could be detected. Comparison of ^{1}H ENDOR spectra of the 2,3,5,6-tetra-methyl-1,4-benzoquinone anion radical in frozen solution, performed both at W-band and at X-band frequency, demonstrated the limitations of achieving orientation selected ENDOR spectra from X-band experiments on systems with small *g*-anisotropy.

1. Introduction

In recent years, several laboratories have started to explore the potential of electron nuclear double resonance (ENDOR) at field/frequency ranges higher than Q-band (35 GHz microwave (MW) frequency, 1.2 T magnetic field),[1−5] and several applications in the fields of biophysics[6−8] and solid-state physics[9] have been reported. In W-band, the increase of the Zeeman energy, which is proportional to the static external magnetic field $\mathbf{B}_0$, in principle, will lead to a higher spectral resolution in the electron paramagnetic resonance (EPR) spectra of radicals and radical pairs.[10−12] For instance, when studying organic radicals with typically small *g*-anisotropies or *g*-differences in the orders of 10^{-4} to 10^{-3}, the increase of $\mathbf{B}_0$ from 0.34 T (X-band) to 3.4 T (W-band) is often necessary to resolve the *g* tensor principal values. For the quinone radical anions studied here, the determination of these *g* tensor components from high-field/high-frequency EPR experiments and their assignments to the molecular axis system has already been described;[10,13] see Figure 1 (top).

Dipolar and quadrupolar hyperfine (HF) interactions, which often contain more specific information of the system than the *g* tensors, are field independent. Nevertheless, some important advantages of high-field/high-frequency ENDOR with regard to HF information can often be achieved that are related to the $\mathbf{B}_0$-dependent electron or nuclear Zeeman interactions:

(i) Overlapping signals, occurring, for example, in ENDOR spectra from different nuclei with different nuclear Larmor frequencies, can often be separated at higher field/frequency ranges.

(ii) For biological systems, where radicals with small *g*-anisotropies ($\leq 10^{-3}$), such as quinones or tyrosines, are involved, high-field experiments allow the measurement of "single-crystal-like" ENDOR spectra even on randomly oriented samples.[6]

At X-band, orientation-selective ENDOR experiments require a much larger g-anisotropy, as is typical for transition metal complexes.[14−17] In this publication, a comparison of orientation-selective ENDOR measurements on the duroquinone (DQ) anion radical in frozen alcoholic solution, performed at X-band as well as W-band, demonstrates that a unique interpretation of the HF data from X-band ENDOR often cannot be achieved.

* To whom correspondence should be addressed.
† Institut für Experimentalphysik.
§ Max-Volmer-Institut für Biophysikalische Chemie und Biochemie.
‡ Present address: Institut für Physikalische und Theoretische Chemie, Universität Frankfurt, Marie-Curie Strasse 11, D-60439 Frankfurt, Germany.
△ Present address: Section de Bioénergétique, Departement de Biologie Cellulaire et Moleculaire, CEA-Saclay, F-91191 Gif-sur-Yvette, Cedex, France.
¶ Present address: Max-Planck-Institut für Biophysik, Heinrich-Hoffmann-Strasse 7, D-60528 Frankfurt, Germany.

S1089-5647(98)00510-0 CCC: $15.00
Published on Web 05/14/1998

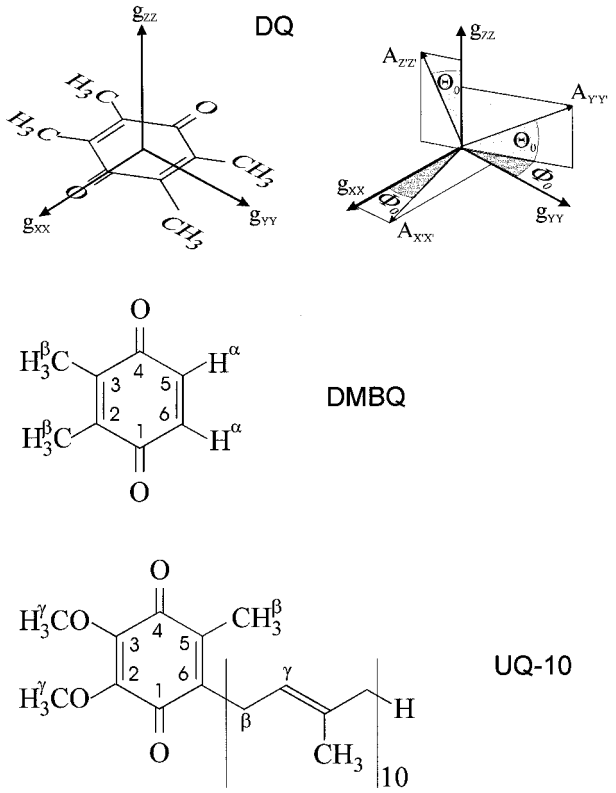

Figure 1. Structural formulas of the investigated quinones: (Top) 2,3,5,6-Tetramethyl-1,4-benzoquinone (duroquinone, DQ) with *g* tensor principal axes system that coincides with the molecular axes.[10] The angles Θ_0 and Φ_0 indicate relative orientations of the HF tensors with respect to the *g* tensor principal axes system. (Center) 2,3-Dimethyl-1,4-benzoquinone (DMBQ) with numbering scheme. (Bottom) 2,3-Dimethoxy-5-methyl-6-(decaprenyl)-1,4-benzoquinone (ubiquinone-10, UQ-10). Note that in this work, hydrogens directly attached to the quinone ring are called α-protons, hydrogens one bond away from the π-system are β-protons, etc.

Here we present first W-band ENDOR measurements on ubiquinone-10 radical anions (UQ-10$^{-\bullet}$) in vitro and in vivo and some related model systems. UQ-10 is found in many biological processes; for example in reaction centers (RCs) of photosynthetic bacteria where it serves as an electron acceptor.[18] In the RC of *Rhodobacter (Rb.) sphaeroides*, two UQ-10 molecules (Q_A and Q_B) act in sequence in the light-induced electron transport chain. These quinones have different redox potentials; Q_A accepts only one electron and no protons whereas Q_B can be doubly reduced and protonated to form the hydroquinone like that found for quinones in solution.[19] The unusual properties of Q_A in the RC must result from a specific binding site in the protein that is quite different from that of Q_B (for X-ray data see ref 20). It has been proposed that asymmetric H bonds to $Q_A^{-\bullet}$ are responsible for this effect.[21−25] So far, no final conclusions about the strengths of the H bonds[21] and, in particular, about their directions could be obtained.

In this work W-band ENDOR measurements on $Q_A^{-\bullet}$ in RCs of *Rb. sphaeroides* in which the native Fe^{2+} was replaced by Zn^{2+} (ZnRCs) are presented. As was shown earlier, this replacement decouples $Q_A^{-\bullet}$ ($S = 1/2$) from the high-spin Fe^{2+} ($S = 2$) and allows one to observe a narrow EPR line of the semiquinone anion radical.[26] The EPR/ENDOR data are compared with those obtained from UQ-10$^{-\bullet}$ in 2-propanol solution. The orientation-selective ENDOR measurements yield insight into details of the electronic structure of $Q_A^{-\bullet}$ and its surrounding and complement earlier results obtained by X-band EPR/ENDOR of frozen ZnRC solutions[21,27] and of ZnRC single crystals.[28,29]

2. Experimental Section

2.1. Instrumentation. The laboratory-built pulsed W-band EPR/ENDOR spectrometer has been described in ref 4. It operates at a Zeeman magnetic field of 3.4 T and W-band MW frequencies of ∼95 GHz. The cylindrical single-mode MW cavity (TE_{011} mode) described in ref 2 was altered to allow in situ illumination of photosensitive samples via a light pipe. Improvements of the RF circuit which allow the application of nuclear magnetic resonance (NMR) fields with high efficiency and linearity at the sample, were outlined in ref 6.

All W-band ENDOR spectra were recorded with the Davies-ENDOR pulse sequence,[30] consisting of three MW pulses and one RF pulse following the first MW pulse. The MW π pulse inverts the electron Boltzmann spin polarization and is followed by a mixing period T_M. Within T_M, an RF π pulse is converting the longitudinal electron-spin polarization to electron-nuclear two-spin order when the RF frequency is resonant with a nuclear transition. This effect is detected by conversion to electron single-quantum coherence by a MW two-pulse echo sequence. The ENDOR spectrum is obtained in absorption as change of the echo intensity when sweeping the RF frequency.

Although the more common continuous wave (CW) ENDOR technique could have been used as an alternative to obtain the W-band ENDOR spectra,[6] we chose the pulsed method because of its technical advantages as a more stable mode of ENDOR operation: the main advantage compared with the CW mode is the absence of any irradiation of the sample while detecting the echo amplitude. In particular, the high-power RF radiation in the frequency range of 140 ± 20 MHz produces distortions caused by stray fields and heating effects of the continuously powered NMR coil, thus making the CW ENDOR experiments at W-band rather difficult. In contrast, the pulsed ENDOR mode offers a stable, MW- and RF-silent way of signal detection, with negligible heating of the NMR coil due to an RF duty cycle of only 0.1% at a repetition rate of 200 Hz. The W-band ENDOR spectra were recorded in 20 kHz steps, with 400 or 1000 acquisitions per step, resulting in total accumulation times between 23 and 83 min for each spectrum.

The mixing period T_M, in which the RF pulse is applied, has to be short compared with the nuclear and electronic longitudinal relaxation times (T_1). The spectra shown here were taken with 6-μs RF-π, 80-ns MW-π/2, and 160-ns MW-π pulses, respectively. At the applied temperatures of 115 ± 5 K, the electronic T_1 of quinone radicals is in the order of 400 to 600 μs, whereas the nuclear T_1 lies in the millisecond range. This fully meets the requirements of long longitudinal relaxation times T_1 compared with the mixing time T_M.

2.2. Spectral Analysis. For doublet-state systems, the spin Hamiltonian can be written as:

$$\hat{H} = \mu_B \mathbf{B}_0 \underline{g} \hat{\mathbf{S}} + h \sum_{i=1}^{n} \hat{\mathbf{S}} \underline{A}^{(i)} \hat{\mathbf{I}}_i - g_N \mu_N \mathbf{B}_0 \sum_{i=1}^{n} \hat{\mathbf{I}}_i \qquad (1)$$

in which $\underline{A}^{(i)}$ is the HF tensor of nucleus *i* or a group of equivalent nuclei, μ_B and μ_N are the Bohr and the nuclear magneton, respectively, *h* is Planck's constant, $\hat{\mathbf{S}}$ is the electron spin operator, $\hat{\mathbf{I}}_i$ is the nuclear spin operator, $\underline{g}$ is the *g*-tensor, and g_N is the nuclear *g*-factor.

The EPR spectra of radicals in frozen solutions (and powder samples) result from superpositions of EPR signals from all

molecular orientations with respect to the magnetic field.[31] Under certain circumstances − which depend on the magnitude of $\mathbf{B}_0$, the *g*-anisotropy, and the inhomogeneous line width caused by unresolved HF couplings − each field position in the EPR spectrum represents a specific manifold of relative molecular orientations from the entire orientational distribution. This information can be used to perform ENDOR and thereby to select the corresponding set of orientations. If the EPR spectrum is dominated by the *g*-anisotropy (i.e. anisotropic Zeeman interaction $\Delta g\mathbf{B}_0 \gg$ inhomogeneous line width ΔB), even single-crystal-like ENDOR spectra can be obtained at the turning points of the EPR spectrum and HF tensors can be elucidated with respect to the g-tensor principal axes system.[16] However, even for EPR spectra resulting from well-resolved rhombic *g*-tensors with $g_{11} \gg g_{22} \gg g_{33}$, a selection of a finite solid angle of relative molecular orientations is only possible at the turning points (g_{11} and g_{33}), whereas at all intermediate field positions including g_{22}, a broad, but still well-defined selection of orientations will occur.

If the inhomogeneous line width caused by the unresolved anisotropic HF couplings cannot be neglected compared with the *g*-anisotropy, orientation selection may occur as a result of both the HF *and* the Zeeman terms in eq 1. This additional contribution to the orientational selection can be taken into account in the data analysis by a rigorous simulation of powder ENDOR spectra. However, to obtain information about the relative orientations of HF tensors with respect to that of the *g*-tensor from powder ENDOR spectra, the requirement $\Delta g\mathbf{B}_0 > \Delta B$ must be fulfilled.

The simulation program used here takes into account both HF and Zeeman anisotropies, and was described in more detail in ref 6. After transformation of the predicted HF tensors $\underline{A}^{(i)}$ into a reference system, which is given by the *g*-tensor principal axes system, the EPR spectrum is calculated by the orientation-dependent field positions $B_{res}(\Theta,\Phi)$ for all relative molecular orientations with spherical angles Θ and Φ, by

$$B_{\mathrm{res}}(\Theta,\Phi) = \frac{(\nu - A^{(i)}(\Theta,\Phi)m_{\mathrm{i}})h}{g(\Theta,\Phi)\mu_{\mathrm{B}}} \qquad (2)$$

where ν is the excitation MW frequency, m_i are the magnetic spin quantum numbers of the nuclei, and $g(\Theta,\Phi)$ and $A^{(i)}(\Theta,\Phi)$ are the angle-dependent *g* and HF values, respectively. The complete nuclear configurations, including multiplets for up to six different HF tensors with up to 12 equivalent nuclei each, are taken into account with their statistical weights. Two Euler angles, describing the relative orientation for each HF tensor with respect to the *g*-tensor reference system, are used. Throughout this paper we use the following notation: the axes system of the *g* tensor is X, Y, Z; the axes system of the HF tensor is X′, Y′, Z′. The two axes systems, including the two Euler angles, are visualized in Figure 1 (top). The angle Φ_0 is the one between the projection of the HF principal symmetry axis (Y′) onto the molecular plane and the Y-axis of the *g*-tensor axes system, which corresponds to the angle between the X- and X′-axes. The angle Θ_0 is the tilt angle of the Y′-axis out of the molecular plane, which corresponds to the angle between the Z- and the Z′-axes. By taking into account these two Euler transformations in the calculation, all axially symmetric HF tensors may be oriented in any possible relative direction with respect to the reference system. The treatment still remains correct for HF tensors that deviate significantly from axial symmetry as long as there is no evidence for a strong (>15°) additional 'rotation' of the HF tensor principal axes system around its dominant (Y′) axis. For cases where only small deviations from axial symmetry are observed (such as for the HF tensor for H_α of DMBQ as described later), it can easily be rationalized that the third transformation can safely be neglected for simulations even of the highly orientational selective W-band ENDOR spectra.

To find the angular selection for a chosen spectral EPR position, B_{ENDOR}, the entire EPR spectrum is first simulated by taking into account all molecular orientations. ENDOR transition frequencies are only calculated for all those molecules that contribute to the EPR spectrum at B_{ENDOR} within a variable interval representing the homogeneous EPR line width. The respective contribution of any transition is convoluted with a Lorentzian line shape function, reflecting the spectral offset of its field position from B_{ENDOR}. Also, the statistical weight of each transition due to its configurational origin (EPR multiplets) is taken into account for the integration of the ENDOR spectra. The ENDOR frequencies ν_{ENDOR} are determined for the W-band simulations in the high-field approximation by

$$\nu_{\mathrm{ENDOR}}^{(i)} = \left| \frac{g_{\mathrm{N}}\mu_{\mathrm{N}}B_0}{h} - m_{\mathrm{s}}A^{(i)}(\Theta,\Phi) \right| \qquad (3)$$

whereas X-band ENDOR simulations were treated by a more general expression.[6,15] Convolution with Lorentzian or Gaussian line shapes can be chosen with different line widths and relative amplitudes for each HF coupling in the ENDOR simulation. According to the origin of the ENDOR line shapes (inhomogeneous broadening), convolution with a Gaussian function in general led to better agreement with the experimental spectra and was chosen for most of the ENDOR simulations. In contrast, the Lorentzian line shape function led to better results for simulations of spectra taken at the g_{ZZ} position, where the highest orientation selectivity is achieved and the ENDOR lines can almost be regarded as homogeneous. The line widths were set empirically to fit the experimental spectra. No attempt was made at this stage to fully determine the line widths and relative amplitudes analytically in the orientation-selective ENDOR spectra. In addition to the orientational selectivity just described, line widths and amplitudes are further influenced by several other factors. Prominent influences to the ENDOR amplitudes are, for example, given by experimental conditions such as the HF-dependent selectivity of the Davies ENDOR experiment. This selectivity has been described by Hoffman et al.[17] in terms of a selectivity parameter $\zeta = At_{\mathrm{p}}$, where *A* is the measured HF coupling and t_{p} is the length of the applied MW π pulse.[17] Based on this relation and using $t_{\mathrm{p}} = 150$ ns for the MW inversion π pulses in our W-band ENDOR experiments, one can estimate that signals from HF couplings <1 MHz are strongly reduced in their relative amplitudes. Nevertheless, smaller couplings can still be observed in the ENDOR spectra in principle. In part, this effect is compensated for in the simulations by choosing the appropriate relative intensity parameter for small HF couplings. Furthermore, relative intensities and amplitudes of ENDOR signals from different groups of nuclei are influenced by differences of their nuclear spin relaxation times, which can vary for different HF couplings. Changes of the spin relaxation times, dependent on the applied Zeeman field, can also lead to broader ENDOR lines at W-band as compared with X-band.

The effect of "HF-enhancement", which results in larger amplitudes of the ENDOR lines above the nuclear Larmor frequency, is naturally less pronounced at W-band frequencies, see Figures 2 and 3.

The selected manifolds of molecular orientations can be represented graphically for each ENDOR simulation (see Figures

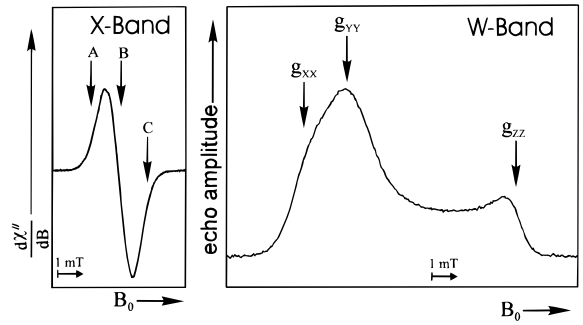

Figure 2. EPR spectra of $DQ^{-\bullet}$ in frozen IP-D_8 ($T = 115$ K), recorded at X-band (9.5 GHz, 0.34 T) in CW detection (first-derivative) mode (left) and at W-band (95 GHz, 3.4 T) in field swept 2-pulse echo-detection mode (right). The π − pulse length was 90 ns and the pulse separation time τ was 140 ns. The scaling of the field axes is identical in both spectra. In the W-band spectrum, the field positions representing the *g* tensor principal values are labeled. In the X-band spectrum, the field positions A and C indicate ± 1 mT field variations from the central position labeled B.

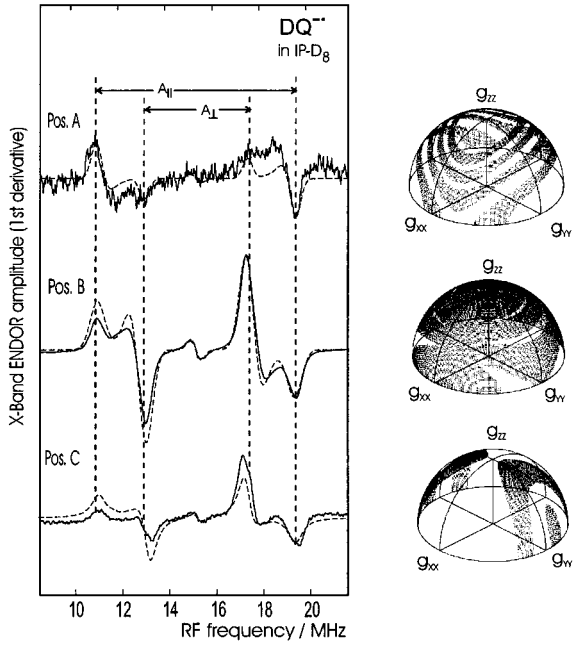

Figure 3. (Solid lines) First-derivative X-band ENDOR spectra of $DQ^{-\bullet}$ in frozen solution of IP-D_8 ($T = 115$ K). The spectra were recorded in the CW mode at the field positions A, B, and C, as indicated in Figure 2. (Dashed lines) Simulations of the spectra as described in the text. (Right) Representation of orientation selections as determined from the simulations (for details, see *Data Analysis* section).

3 to 6). Note that the relative weighting for each single angular selection with angles Θ and Φ as well as the number of transitions contributing to each particular orientation are not visible in this representation. Furthermore, the depicted distributions are restricted by a preset lower limit of their respective relative statistical weights for the entire ENDOR spectrum. Orientations from transitions that contribute <15% of the maximum possible value of the transition are not shown, although they are included in the simulation of the spectra. These graphical representations, in addition to the general visualization of the orientational selectivity of the ENDOR spectra, reflect the influence of different HF broadenings on the angular selectivity. Even the multiplicity of the HF patterns can be seen if no overlap of different HF tensors occurs (e.g., the 13 EPR lines from the 12 equivalent nuclei are reflected in the orientation selection shown for $DQ^{-\bullet}$ in Figure 4).

2.3. Sample Preparation. *Semiquinone Anion Radicals in Frozen Solutions.* 2,3,5,6-Tetramethyl-1,4-benzoquinone (duroquinone, DQ), 2,3-dimethyl-1,4-benzoquinone (DMBQ), and 2,3-dimethoxy-5-methyl-6-decaprenyl-1,4-benzoquinone (ubiquinone-10, UQ-10) (see Figure 1) were obtained from Aldrich. DQ and DMBQ were purified by sublimation prior to use. The quinones were dissolved either in fully deuterated (IP-D_8) or protonated (IP-H_8) 2-propanol (concentrated $\approx 2 \times 10^{-3}$ M). The semiquinone anion radicals were generated from the parent quinone by adding a slightly basic potassium-*tert*-butylate (K−*t*-BuO) solution in the respective solvent to the sample.[10,32] The solution was deoxygenated by bubbling with purified argon for a few minutes and then rapidly frozen in the gas-flow cooling system of the spectrometer. Deoxygenating of the quinone solution was accomplished in the sample quartz tube (0.7−0.9-mm outer diameter, 0.02-mm wall thickness) using thin glass capillaries with ≈0.2 mm diameter, which were fed into the sample tube. This process was done before, during, and after the generation of the radicals, which was achieved by adding the reductant solution directly into the sample tube. Sample volumes were between 10 and 15 μL. The freezing time in the precooled magnet bore was typically <3 min.

Q_A in Reaction Centers from Rb. sphaeroides. To remove the electron-spin coupling to the high-spin Fe^{2+} in the RC,[33] the Fe^{2+} was replaced by Zn^{2+} (ZnRC). To facilitate the $Fe^{2+} \rightarrow Zn^{2+}$ exchange, the mutant HC(M266), which was described earlier,[34] was used. In this procedure ZnRCs were obtained biosynthetically by growing the mutants in high Zn/low Fe media. An incorporation of ≥90% Zn was obtained. The ZnRC's exhibited very similar electron-transfer kinetics as native FeRC's.[29,35]

Photogeneration of the Q_A anion radical in the RCs was accomplished with light from a solid-state CW laser (30 mW power, 790 nm wavelength) that was coupled to the cavity via a quartz fiber. A saturated sodium ascorbate solution was added (10%) to reduce the photogenerated $P^{+\bullet}$, thereby avoiding the detection of the radical pair state $P^{+\bullet}Q^{-\bullet}$. The sample was illuminated while slowly freezing, allowing for the stable $Q_A^{-\bullet}$ to be accumulated in the frozen matrix.

4. Results and Discussion

4.1. Duroquinone (DQ). In Figure 2, X- and W-band EPR spectra of $DQ^{-\bullet}$ are shown. The X-band spectrum is recorded in CW mode, using field modulation and phase-sensitive detection. Accordingly, the spectrum is shown as the first derivative. The W-band spectrum shows the field-dependent, electron-spin-echo amplitude (ESE-detection), recorded with a $\pi/2-\tau-\pi$ MW pulse sequence. Although at X-band frequencies no indications of *g*-anisotropy can be resolved, this is clearly accomplished at W-band frequencies because of the 10 times larger Zeeman field.

The W-band EPR spectrum shows significant deviations from a familiar Pake powder pattern;[31] that is, the local minimum visible between the g_{yy} and g_{zz} positions in the W-band spectrum is a result of anisotropic motional processes that occur on the time scale of the pulsed EPR experiment. Such anisotropic transverse spin relaxation (T_2) effects observable by pulsed high-field EPR provide interesting information about slow-motional dynamics that are not accessible by other spectroscopic techniques.[36,37]

To determine the anisotropic HF interactions in $DQ^{-\bullet}$ between the 12 protons of the four magnetically equivalent methyl groups and the unpaired electron, orientation-selective ENDOR measurements were performed at different field positions of the EPR spectra. The field positions are marked by arrows in Figure 2.

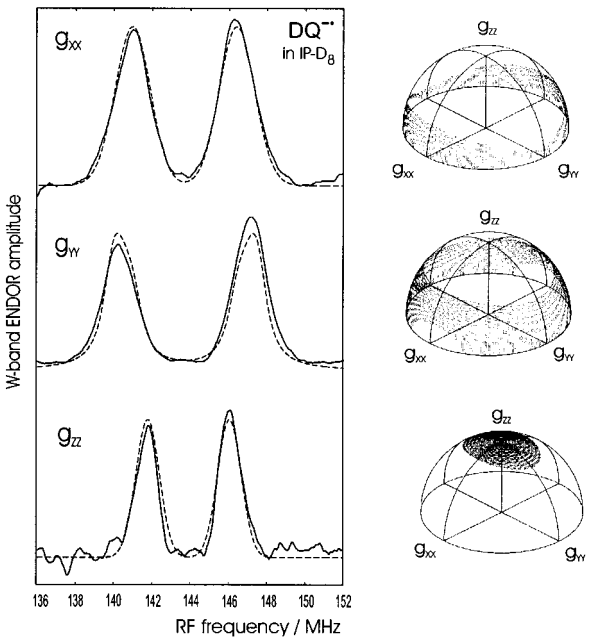

Figure 4. (Solid lines) W-Band ENDOR spectra of $DQ^{-\bullet}$ in frozen solution of IP-D_8 ($T = 115$ K). The spectra were recorded with the Davies-ENDOR pulse sequence at field positions corresponding to the canonical values of the g tensor g_{xx}, g_{yy}, and g_{zz} as indicated in Figure 2. (Dashed lines) Simulations of the spectra as described in the text. (Right) Representation of orientation selections as determined from the simulations (for details, see *Data Analysis* section).

From temperature-dependent ENDOR measurements at X-band it is known that the methyl groups rotate freely at temperatures >90 K.[32,38] Accordingly, in the case of fast rotation compared with the microseconds observation time scale, each methyl group exhibits only one HF tensor that is expected to be axially symmetric with its symmetry axis in the molecular plane. The associated HF component, $A_{||}$, is expected to be oriented approximately along the $C-CH_3$ bond direction.

In Figure 3, first-derivative CW ENDOR spectra, recorded at X-band at three different spectral positions (A, B, and C; see Figure 2, left), are shown. The ENDOR spectrum taken at the central EPR position B displays a line shape typical for a powder distribution of an almost axially symmetric HF tensor. From this spectrum, principal components of the methyl HF tensor are obtained ($A_{||} = 7.9$ MHz and $A_{\perp} = 4.4$ MHz), from which one obtaines $A_{iso} = 5.6$ MHz according to

$$A_{iso} = 1/3\ \mathrm{Tr}(A) = (2\,A_{\perp} + A_{||})/3 \qquad (4)$$

This value is in reasonable agreement with the isotropic value A_{iso} of 5.33 MHz, measured by liquid solution ENDOR.[21,32]

The ENDOR spectrum obtained by saturating the EPR at field position A shows an increased relative signal amplitude of the lines assigned to the $A_{||}$ component. This result indicates that for this EPR field value, molecular orientations are mainly selected with large HF components parallel to $\mathbf{B}_0$. The ENDOR spectrum taken at EPR position C also shows a relative increase of the larger HF component ($A_{||}$), although the effect is less pronounced in this case. Taking into account the considerations already given and the molecular scheme in Figure 1, these assignments lead to contradictions: The $A_{||}$ component, which represents only one of the three HF principal values, cannot be found as a pronounced value along two different Cartesian orientations, as selected by the two g-tensor principal orientations g_{xx} and g_{zz}. Alternatively, the larger HF value could be assigned to $A_{\perp}$, which would, however, be inconsistent with the isotropic value, A_{iso}, found by liquid solution ENDOR.

TABLE 1: Principal Values [MHz] and Orientations of the Methyl Proton HF Tensor of $DQ^{-\bullet}$ in IP-D_8[a]

assignment	$A_{X'X'}$	$A_{Y'Y'}$	$A_{Z'Z'}$	1/3 Tr (A)[b]	Φ_0	Θ_0
CH_3[c]	(+) 4.8(4)	(+) 7.9(4)	(+) 4.2(2)	(+) 5.6(2)	17(5)[o]	0(5)°
CH_3[d]	(+) 4.4(2)	(+) 7.9(2)	(+) 4.4(2)	(+) 5.7(2)	—[e]	—[e]
CH_3[f]	(+) 4.4(1)	(+) 7.5(1)	(+) 4.4(1)	(+) 5.4(1)	—[e]	—[e]

[a] Numbers in brackets are errors in the last digit; the primed axes system refers to the principal axes system of the HF tensor; for definition of angles Φ_0 and Θ_0, see Figure 1. [b] The value measured in liquid solution is 5.33 MHz.[32] [c] W-Band ENDOR. [d] X-Band ENDOR[32] (in ref 32, the $A_{||}$ value was misprinted). [e] Not determined. [f] In frozen EtOH.[38]

Accordingly, one must conclude that in this example no sufficient orientation selection due to the g-anisotropy is obtained, but rather due to the HF-anisotropy, which obviously exceeds the anisotropy of the electron Zeeman interaction. The simulations of the X-band ENDOR spectra, which are based on the results of the W-band ENDOR measurements described later, clearly confirm this assumption. In summary, it has to be noted that for the field settings A, B, and C, the orientational selectivity in X-band ENDOR is rather poor because of the comparable magnitude of HF broadening and g-anisotropy.

The corresponding W-band ENDOR spectra of $DQ^{-\bullet\bullet}$, recorded with the Davies ENDOR pulse sequence, are shown in Figure 4. Note that these spectra are in absorption whereas the X-band spectra are in first derivative. The W-band ENDOR spectra clearly show a different selection mechanism than the X-band spectra. Although the W-band ENDOR lines are strongly broadened due to inhomogeneous HF contributions, one can nevertheless obtain a selection of larger HF values at the g_{yy} position as compared with the mean value selected at the g_{xx} position. In addition, even more pronounced, at the g_{zz} position, smaller HF values are measured compared with the other field positions.

These results confirm the prediction of a larger value $A_{||}$ that lies in the molecular plane. In addition to this more qualitative deduction, one can obtain quantitative results when taking into account rigorous data analysis by simulation of the powder ENDOR spectra.[6] The results are collected in Table 1, which also contains the isotropic HF constant, as measured at 200 K, and the in-plane rotation angle Φ_0 of the g and HF tensor axes systems.

Based on the molecular symmetry of DQ, one would expect an angle of $\Phi_0 = 30°$ for the largest component of the CH_3 HF tensor that should lie along the $C-CH_3$ bond direction. The deviation observed here is attributed to the effect of unequal next-neighbor spin densities (at C positions C_1 and C_3, for example). This is also the reason for the observed deviation of the CH_3 HF tensor from axial symmetry and for the relatively large anisotropy.[21,32]

4.2. 2,3-Dimethyl-1,4-benzoquinone (DMBQ). In Figure 5, orientation-selective W-band ENDOR spectra of the DMBQ anion radical in frozen deuterated 2-propanol solution are shown. The simulations of the spectra (dotted lines), taken at the three EPR positions (g_{xx}, g_{yy}, and g_{zz}), are also depicted together with the respective orientation selections. Due to the molecular symmetry, the two methyl groups are magnetically equivalent, as are the two α-protons at ring positions 5 and 6.

The isotropic HF constants, as measured by X-band ENDOR in liquid solution, are given in Table 2 together with the results of the W-band ENDOR simulations. The HF values as

TABLE 2: Principal Values [MHz] and Orientations of the Proton HF Tensors of $DMBQ^{-\bullet}$ in IP-D_8[a]

number	assignment	$A_{X'X'}$	$A_{Y'Y'}$	$A_{Z'Z'}$	1/3 *Tr* (*A*)	A_{iso}[b]	Φ_0	Θ_0
1, 1′	CH_3[c]	(+) 4.2(3)	(+) 7.3(2)	(+) 3.6(2)	(+) 5.0(2)	—[d]	22(5)°	0(5)°
	CH_3[e]	(+) 3.7(2)	(+) 7.1(2)	(+) 3.7(2)	(+) 4.8(2)	+4.83	—[d]	—[d]
2, 2′	H_α[c]	(−) 11.0(5)	(−) 0.8(4)[e]	(−) 9.5(5)	(−) 7.1(3)	—[d]	15(6)°	0(5)°
	H_α[e]	(−) 11.1(2)	(−) 0.8(2)	(−) 9.4(2)	(−) 7.1(2)	−7.30	—[d]	—[d]

[a] Numbers in brackets are errors in the last digit; the primed axes system refers to the principal axes system of the respective HF tensor; for definition of angles Φ_0 and Θ_0, see Figure 1; the magnitudes and signs of A_{iso} were determined by ENDOR and general-TRIPLE experiments in liquid solution, respectively; based on this assignment, the signs of the HF tensor components measured in frozen solutions were deduced. [b] From ref 32 at 200 K. [c] W-Band ENDOR. [d] Not determined. [e] X-Band ENDOR.[32]

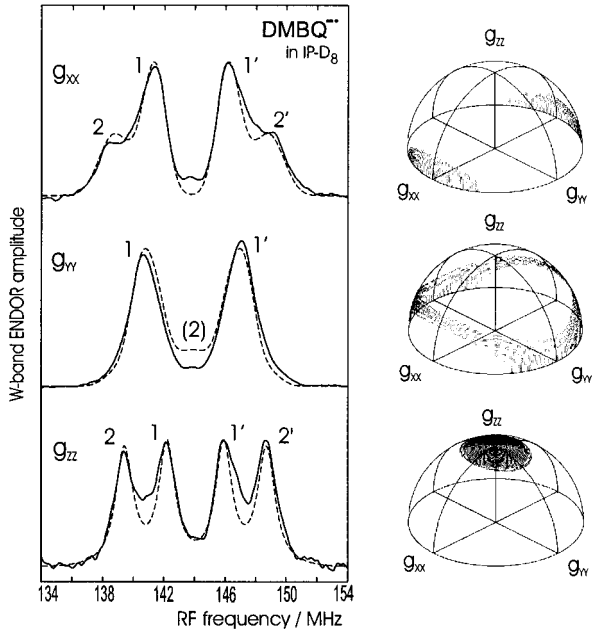

Figure 5. (Solid lines) W-Band ENDOR spectra of $DMBQ^{-\bullet}$ in frozen solution of IP-D_8 (T = 115 K). The spectra were recorded with the Davies-ENDOR pulse sequence at field positions corresponding to the canonical values of the g tensor g_{xx}, g_{yy}, and g_{zz} as shown in Figure 2 for $DQ^{-\bullet}$ (EPR spectrum of $DMBQ^{-\bullet}$ not shown). (Dashed lines) Simulations of the spectra as described in the text. The numbers refer to assignments of spectral positions as given in Table 2 and discussed in the text. (Right) Representation of orientation selections as determined from the simulations (for details, see *Data Analysis* section).

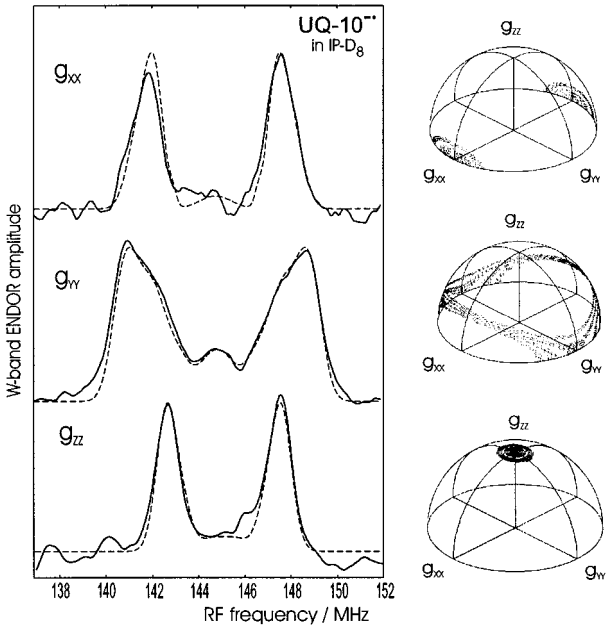

Figure 6. (Solid lines) W-Band ENDOR spectra of $UQ\text{-}10^{-\bullet}$ in frozen solution of IP-D_8 (T = 115 K). The spectra were recorded with the Davies-ENDOR pulse sequence at field positions corresponding to the canonical values of the g tensor g_{xx}, g_{yy}, and g_{zz} as indicated in Figure 2 for $DQ^{-\bullet}$ (EPR spectrum of $UQ\text{-}10^{-\bullet}$ not shown). (Dashed lines) Simulations of the spectra as described in the text. (Right) Representation of orientation selections as determined from the simulations (for details, see *Data Analysis* section).

determined by X-band ENDOR in frozen 2-propanol solution (spectra not shown) are also listed.

The assignment of the CH_3 lines to the respective HF values was basically done by using the methyl HF data from $DQ^{-\bullet}$. Earlier W-band EPR measurements[10] of 1,4-benzoquinone anion radicals in frozen solutions allowed the determination of the α-proton HF components in this system: This gave $|A_{X'X'}|$ = 10.5(6), $|A_{Y'Y'}|$ = 0.9(1), and $|A_{Z'Z'}|$ = 8.7(6) MHz and Φ_0 = 12(5)°,[10] which was in good agreement with RHF−INDO/SP semiempirical MO calculations that resulted in a twist angle of Φ_0 = 14°.[10] The values are similar to those obtained for $DMBQ^{-\bullet}$ (Table 2). The small $A_{||}$- (or $A_{Y'Y'}$) component of $DMBQ^{-\bullet}$, however, cannot be clearly seen in the W-band ENDOR spectrum (Figure 5) because of the broad line width of these W-band ENDOR spectra and probably because of a lack of sensitivity of the Davies ENDOR pulse sequence for small HF couplings (nonselective pulses for small couplings;[17] see section *2.3. Spectral Analysis*).

The additional information obtained by the W-band spectra is the relative orientation (angle Φ_0) of the HF and g tensors, as given in Table 2. Again, the symmetry axes of both HF tensors lie in the molecular plane and deviate somewhat from the C−CH_3 and C−H bond directions because of next-neighbor effects (vide supra). The HF principal values determined from X- and W-band are, within the error margins, in good agreement.

4.3. Ubiquinone-10 (UQ-10). In Figure 6, the W-band ENDOR spectra of $UQ\text{-}10^{-\bullet}$ in frozen solutions of IP-D_8 are shown. As in the previous examples, they were recorded at the "canonical" EPR positions, g_{xx}, g_{yy}, and g_{zz} (as indicated in Figure 2 for $DQ^{-\bullet}$). For $UQ\text{-}10^{-\bullet}$ in deuterated solvent, the dominating ENDOR signals result from the three equivalent protons of the CH_3 group, which rotates freely at temperatures of 110 K. Again, the methyl protons reveal an almost axially symmetric HF tensor with its symmetry axis in the molecular plane. This symmetry axis is expected to be rotated away from the molecular Y-axis by ∼30° as already described for $DQ^{-\bullet}$. This result is confirmed for $UQ\text{-}10^{-\bullet}$ by the simulations of the spectra that agree with the experimental spectra using Φ_0 = 28° (see Table 3). The principal values of the methyl HF tensor are in good agreement with data obtained by X-band ENDOR.[32,39] Angular information is not obtained from the X-band measurements, in which only powder spectra without sufficient orientational selection could be obtained.

The magnitudes of the HF couplings from the CH_2 β-protons and the more remote γ-protons of the isoprenoid substituent have been shown previously to be very sensitive to the orientation of the chain. It is assumed that in frozen solutions,

TABLE 3: Principal Values [MHz] and Orientations of the Proton HF Tensors of UQ-10$^{-\bullet}$ in IP-D_8 and IP-H_8, Including H-bonds (HB)[a]

number	assignment	$A_{X'X'}$	$A_{Y'Y'}$	$A_{Z'Z'}$	1/3 *Tr* (*A*)	A_{iso}[b]	Φ_0	Θ_0
1, 1′	CH_3[c]	(+) 4.8(2)	(+) 8.5(2)	(+) 4.7(2)	(+) 6.0(2)	—[d]	28(4)°	0(4)°
	CH_3[e]	(+) 4.8(1)	(+) 8.5(1)	(+) 4.8(1)	(+) 6.0(1)	+6.00(1)	—[d]	—[d]
2, 2′	HB1[c]	(−) 1.2(3)	(+) 6.3(3)	(−) 1.2(3)	(+) 1.3(3)	—[d]	81(4)°	38(4)°
	HB1[e]	(−) 1.3(1)	(+) 6.0(1)	(−) 1.3(1)	(+) 1.1(1)	—[d]	—[d]	30−60°
3, 3′	HB2[c]	(−) 1.0(3)	(+) 5.2(3)	(−) 1.0(3)	(+) 1.1(3)	—[d]	10(4)°	12(4)°
	HB2[e]	(−) 1.2(1)	(+) 5.6(1)	(−) 1.2(1)	(+) 1.1(1)	—[d]	—[d]	30−60°

[a] Numbers in brackets are errors in the last digit; the primed axes system refers to the principal axes system of the respective HF tensor; for angles Φ_0 and Θ_0, see Figure 1; for signs of HFCs see Table 2. [b] From ref 21 at 200 K. [c] W-Band ENDOR. [d] Not determined. [e] X-Band ENDOR.[32]

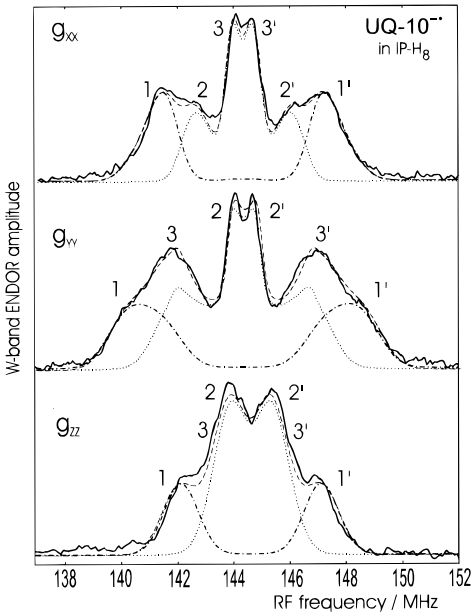

Figure 7. (Solid lines) W-Band ENDOR spectra of UQ-10$^{-\bullet}$ in frozen solution of IP-H_8 (T = 115 K). The spectra were recorded with the Davies-ENDOR pulse sequence at field positions corresponding to the canonical values of the g tensor g_{xx}, g_{yy} and g_{zz} as shown in Figure 2 for DQ$^{-\bullet}$ (EPR spectrum of UQ-10$^{-\bullet}$ not shown). For orientational selections, compare Figure 6. (Dashed lines) Simulations of the complete spectra as described in the text. (Dash−dotted lines) Simulations of the methyl HF tensor alone as shown in Figure 6. (Dotted lines) Simulations of the two dominating HF lines ascribed to hydrogen-bonded protons as discussed in the text. The numbers refer to assignments of spectral positions as given in Table 3 and discussed in the text.

the corresponding molecular fragments exhibit a broad distribution of configurations with random relative orientations.[21,32] Therefore, the respective lines are expected to be broadened and difficult to detect in the ENDOR spectra.

In Figure 7, orientation-selected W-band ENDOR spectra of the anion radical of UQ-10 in protonated 2-propanol are depicted. The spectra differ significantly from those in deuterated solvent under otherwise the same experimental conditions. This difference can be used to distinguish between local HF interactions and intermolecular (dipolar) interactions of the unpaired electron with nuclei of the solvent matrix that show up in spectra of immobilized radicals. Similar experiments have been performed earlier at X-band,[32] where two different types of H-bonds could be detected. For UQ-10$^{-\bullet}$ the dominating interactions were identified as axially symmetric HF tensors with isotropic contributions of ∼1 MHz.

The simulations of the W-band ENDOR spectra are shown in Figure 7. In addition to the simulations of the complete spectra (dashed lines), the simulated "difference spectra" are also shown (see figure caption). Thereby, the intra- and intermolecular spectral features are separated and visualized. The simulations of the signals from intermolecular interactions fit the experimental W-band spectra with similar principal values as predicted from X-band ENDOR (see Table 3). However, the orientation of the symmetry axis of the interactions [i.e., the direction of one of the large H-bonds (HB2)], differs from the one predicted from X-band ENDOR and Q-band EPR measurements on powder samples. From these measurements, the symmetry axes of both dominating intermolecular HF tensors were ascribed to out-of-plane H-bonds.[32] From the highly orientation-selective W-band ENDOR spectra, however, we conclude that one of the H-bonds is oriented almost in the quinone plane. This result is evident from the fact that for spectra recorded at both the g_{xx} as well as at the g_{yy} positions, strong additional lines, which must be interpreted as the in-plane components, are detected. Furthermore, the W-band ENDOR data strongly suggest that this in-plane H-bond (HB2) is oriented closely to the g_{yy} axis. In contrast, for the other H-bond (HB1), an out-of-plane angle of 38° and an orientation of its projection onto the molecular plane of 9° with respect to the C−O bond axis (which corresponds to Φ_0 = 81°) are determined.

From the purely dipolar HF tensor components A'_i of the HF couplings to protons in the H-bonds one can estimate the H-bond distance r_{OH} between the hydrogen and the spin-carrying carbonyl oxygen by using the simple point−dipole approximation

$$A'_i(\alpha) = \frac{79\rho_O^{\pi}}{r_{OH}^3}(3\cos^2\alpha - 1) \qquad (5)$$

where A'_i is the dipolar HFC in MHz, ρ_O^{π} is the unpaired spin density at the oxygen, and α is the angle between the applied field, $\mathbf{B}_0$, and the line joining the proton and the oxygen. The principal values of the dipolar HF tensor are then given for α = 0° ($A_{||}$) and α = 90° ($A_{\perp}$) with $A_{||} = 2\,|A_{\perp}|$. The oxygen π-spin density was determined from ^{17}O HF data to be 0.20(2).[32,40] Using this value, one obtains for UQ-10$^{-\bullet}$ in frozen 2-propanol from the H-bond HFCs given in Table 3 the two H-bonds lengths: $r_{OH}^{(1)}$ = 1.8(1) Å and $r_{OH}^{(2)}$ = 1.9(1) Å. Thus, the H-bond strengths are very similar and the lengths are quite typical for quinone radical anions in alcoholic solutions.

It is known from EPR/ENDOR experiments of simple 1,4-benzoquinone radical anions that H-bonds prefer to be oriented in the plane of the quinone molecule.[32,39] An out-of-plane orientation is, however, often obtained when all four positions at the quinone ring are substituted. The detection of one H-bond that lies almost in-plane for UQ-10$^{-\bullet}$ could be a consequence of the rotational freedom of the methoxy groups in this molecule.[25]

4.4. $Q_A^{-\bullet}$ in RCs of *Rb. sphaeroides.* In Figure 8, W-ENDOR spectra of $Q_A^{-\bullet}$ in ZnRCs of the mutant HC(M266) of

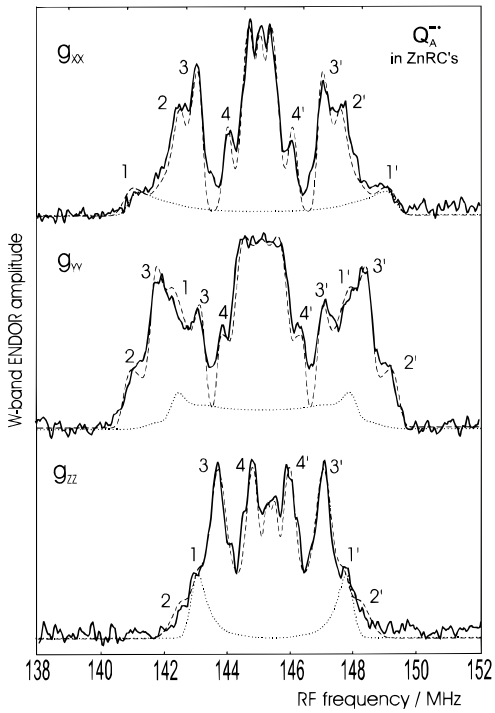

Figure 8. (Solid lines) W-Band ENDOR spectra of $Q_A^{-\bullet}$ in ZnRCs of the mutant HC(M266) of the reaction centers of *Rb. sphaeroides* (T = 115 K). The spectra were recorded with the Davies-ENDOR pulse sequence at field positions corresponding to the canonical values of the g tensor g_{xx}, g_{yy}, and g_{zz} as indicated in Figure 2 for $DQ^{-\bullet}$ (EPR spectrum of $Q_A^{-\bullet}$ not shown). For orientational selections, compare Figure 6. (Dashed lines) Simulations of the complete spectra as described in the text. (Dotted lines) Simulations of the dominating H-bond HF lines as discussed in the text. The numbers refer to assignments of spectral positions as given in Table 4 and discussed in the text.

Rb. sphaeroides are shown. The spectra were recorded at the canonical positions of the EPR spectrum, corresponding to the principal values of the g tensor.

The complexity of the ENDOR spectra of $Q_A^{-\bullet}$ in RCs leads to partially overlapping lines, which makes the interpretation of the spectra rather difficult, as compared with UQ-$10^{-\bullet}$ in vitro (Figures 6 and 7). It has been shown by ENDOR at X-band frequencies on frozen solutions[21,27] and single crystals[28,29] that the HF components can be shifted by up to 25% compared with the in vitro values. Therefore, one has to be cautious when using the values found for the system in frozen alcoholic solution as input data for the simulation of the in vivo spectra.

The simulation of the W-band ENDOR spectra has been attempted by taking the HF tensor of the CH_3 group from previous X-band ENDOR studies on ZnRC HC(M266) single crystals[29] as a starting point. In this work, another large hydrogen hyperfine coupling (H HFC) could be detected and assigned to one methylene (CH_2) proton which, in contrast to UQ-$10^{-\bullet}$ in frozen 2-propanol, is expected to show up clearly for $Q_A^{-\bullet}$ in the RC due to the well-defined orientation of the isoprenoid chain in the protein.

The results of our simulations are shown in Figure 8. Four different HF tensors could be assigned (labeled 1,1′ to 4,4′), which are summarized in Table 4. The magnitude and orientation of the methyl HF tensor is in very good agreement with the single-crystal studies.[29] It is remarkable that for $Q_A^{-\bullet}$ a significantly smaller CH_3 HF tensor is obtained than for UQ-$10^{-\bullet}$ in alcoholic solution (compare data in Tables 4 and 3). This shift of spin density in the quinone ring has been traced back to an asymmetric binding situation of $Q_A^{-\bullet}$ in the protein pocket of the RC and could be explained by a difference in the strengths of H-bonds between specific amino acid residues and the two carbonyl oxygens of the quinone (vide infra).[21]

The HF data assigned to one of the two CH_2 protons are also in good agreement with the respective information obtained from the single-crystal rotation patterns,[29] as well as with earlier results obtained from X-band ENDOR measurements on frozen solutions of ZnRCs.[21,27] The $A_{||}$ direction ($A_{Y'Y'}$) of the CH_2 HFC was determined to be $\Theta_0 = 30°$ out of the molecular plane and its projection onto the plane deviated by $\Phi_0 = 5°$ from the molecular Y-axis.

One of the three large HF tensors used for the ENDOR simulations has been assigned to a strong coupling of a hydrogen-bonded proton. This HF tensor deviates from axial symmetry, and yields an isotropic contribution of approximately −0.4 MHz. The largest component ($A_{Y'Y'}$) is oriented out of the molecular plane ($\Theta_0 = 12°$) and its projection onto the plane deviates 15° from the C−O bond direction; that is, the molecular X-axis; this corresponds to $\Phi_0 = 75°$. The principal values of this H-bond HF tensor are in reasonable agreement with values reported from X-band ENDOR studies,[21] where three ENDOR lines at 9.0, 6.4, and 4.7 MHz for $Q_A^{-\bullet}$ in ZnRCs of *Rb. sphaeroides* R26 were measured and identified as signals arising from exchangeable protons.[1]

[In ref 21, the observed splittings were assigned to two axially symmetric H-bonds of different strength. From the W-band ENDOR spectra there is no experimental evidence for the existence of two strong H-bonds (i.e., one strong HF tensor that deviates from axial symmetry is very suitable for the simulations of the spectra). This interpretation is also in agreement with the X-band ENDOR spectra from ref 21. Furthermore, McConnell−Strathdee[41] type calculations of the dipolar tensor of hydrogen in a tight H-bond clearly show that the tensor deviates from axial symmetry.]

From Q-band EPR,[22,23] electron−spin−echo envelope modulation (ESEEM),[42,43] and Fourier transform infrared (FTIR) studies,[24,25] performed in part on selectively isotope-labeled quinones in ZnRCs, an asymmetric binding of $Q_A^{-\bullet}$ to the N−H of a histidine was postulated. These studies showed that the strong binding site of the quinone is the oxygen on ring position 4 (Figure 1). This result is further supported by a recent X-ray structure analysis of *Rb. sphaeroides*,[44] which indicates that this carbonyl group is located within H-bond distance to His(M219). Based on these observations it is proposed that the strong H-bond detected in our experiments is between the oxygen O_4 of $Q_A^{-\bullet}$ and the N−H of His(M219). Using an oxygen π-spin density of 0.20, one can estimate from eq 5 a quite short H-bond distance of r_{OH} = 1.5(1) Å. An even lower spin density of 0.15 is estimated[45] from the ^{17}O HFCs detected earlier[21] and leads to r_{OH} = 1.4(1) Å.

The direction of the symmetry axis of the dominating H-bond that is closely oriented to the molecular X-axis is also in agreement with the results of anisotropic transverse relaxation studies by pulsed high-field EPR,[36,37] which clearly show a preference of librational motions of $Q_A^{-\bullet}$ around the C−O symmetry axis.

Several additional sets of ENDOR signals could be distinguished in the W-band ENDOR spectra, from which only the largest one (labeled 4,4′ in Table 4 and Figure 8) has been tentatively assigned so far to a CH_3 HF tensor of one of the methoxy groups. The smaller HF couplings may either result from more remote protons of the isoprenoid chain, or from the

TABLE 4: Principal Values [MHz] and Orientations of the Proton HF Tensors of $Q_A^{-\bullet}$ in ZnRCs of *Rb. sphaeroides* Mutant HC(M266)[a]

number	assignment	$A_{X'X'}$	$A_{Y'Y'}$	$A_{Z'Z'}$	1/3 *Tr* (*A*)	Φ_0	Θ_0
2, 2′	CH_2	(+) 5.0(2)	(+) 8.6(2)	(+) 5.6(2)	(+) 6.4(2)	5(5)°	30(5)°
3, 3′	CH_3	(+) 3.6(2)	(+) 6.8(2)	(+) 3.2(2)	(+) 4.5(2)	25(5)°	0(5)°
1, 1′	H-bond	(−) 5.7(3)	(+) 8.8(3)	(−) 4.4(3)	(−) 0.4(3)	75(5)°	12(5)°
4, 4′	OCH_3	2.0(2)	2.7(2)	1.8(2)	−	8(5)°	0(5)°
−	−	0.6(1)	1.5(2)	1.1(2)	−	−	−
−	−	0.10(5)	0.10(5)	0.20(5)	−	−	−

[a] Numbers in brackets are errors in the last digit; the primed axes system refers to the principal axes system of the respective HF tensor; the assignment of the HF tensor labeled 4, 4′ is only tentatively; the signs of the sets of smaller HF data have not been determined and no specific assignments could be made so far for these couplings.

methyl protons of the other OCH_3 group, or from a weaker H-bond to the carbonyl oxygen O_1 (see Figure 1).

5. Summary and Outlook

Davies-type pulsed high-field ENDOR experiments were performed at 95 GHz (W-band) on randomly oriented semiquinone anion radicals in frozen solutions. Well-resolved, orientation-selective EPR and ENDOR spectra for these systems were obtained. High-field/high-frequency ENDOR was shown to be superior to X-band ENDOR in particular with respect to orientational selection. In addition to the magnitudes of the HF tensors, relative orientations of the tensor axes with respect to the *g* tensor principal axis system were obtained from the simulations of W-band powder ENDOR spectra. This tool has been used to determine H-bond directions, for example for UQ-$10^{-\bullet}$ in frozen alcoholic solution. The primary acceptor radical anion $Q_A^{-\bullet}$ in photosynthetic bacterial RCs was also studied by W-band ENDOR in ZnRCs from the mutant HC(M266) of *Rb. sphaeroides*. Thereby, HF data including information about H-bond directions have been obtained that complemented the data from X-band ENDOR studies of ZnRC single crystals.[29] In particular, the analysis derived from the W-band ENDOR experiments suggests that a strong H-bond to $Q_A^{-\bullet}$ contributes to its unusual properties and hence plays an important functional role in the electron transfer process.

To measure and fully analyze the interactions with all exchangeable hydrogens − probably involved in H-bonds between the quinone and the protein − W-band ENDOR investigations with orientation selection of ZnRCs with deuterated UQ-10/H_2O buffer are envisaged. Specific labeling in particular of the carbonyl groups by ^{13}C and ^{17}O but also of the other substituents would allow measurement of these HF tensors and thus give a more complete picture of the spin density shifts. Furthermore, an investigation of other more symmetric quinones − like DQ − substituted into the A-site of *Rb. sphaeroides* ZnRCs[21] would be well suited to probe the fine details of the symmetry of the binding site.

Much less information than for $Q_A^{-\bullet}$ was obtained so far for the second quinone, $Q_B^{-\bullet}$. This second quinone can be prepared in the RC by a single saturating laser flash in the presence of cytochrome c_2 − or similar donors − that reduce the primary donor cation radical $P_{865}^{+\bullet}$ to P_{865}. So far, the difficulties in generating $Q_B^{-\bullet}$ in the RC have prevented its study in ZnRC single crystals. Here, the W-band ENDOR technique with orientation selection performed on frozen ZnRCs is the method of choice to measure magnitudes and orientations of the HF tensors of $Q_B^{-\bullet}$ and its environment as demonstrated for $Q_A^{-\bullet}$ in this work.

Acknowledgment. The authors are grateful to F. Lendzian (TU Berlin) for making available the McConnell−Strathdee calculations on the dipolar H-bond HF components and for many helpful discussions concerning the assignment of the HF data of $Q_A^{-\bullet}$ in ZnRCs. The mutant HC(M266) was provided by J. P. Allen and J. C. Williams (ASU, Tempe, USA). I. Geisenheimer (TU Berlin) assisted with the RC preparations, which is gratefully acknowledged, as is the helpful advise concerning the ZnRC preparations of the mutant given by E. C. Abresch (U.C. San Diego). We thank J. T. Törring (FU Berlin) who wrote the control program for the ENDOR experiment and interfaced the hardware of the W-band spectrometer. This work was supported by the Deutsche Forschungsgemeinschaft (SFB 337 TP B4, SFB 312 TP A4), NATO (CRG 910468), and Alexander von Humboldt Stiftung (to A.T.G.).

References and Notes

(1) Burghaus, O.; Toth-Kischkat, A.; Klette, R.; Möbius, K. *J. Magn. Reson.* **1988**, *80*, 383.
(2) Burghaus, O.; Rohrer, M.; Götzinger, T.; Plato, M.; Möbius, K. *Meas. Sci. Technol.* **1992**, *3*, 765.
(3) Disselhorst, D. A. J. M.; van der Meer, H.; Poluektov, O. G.; Schmidt, J. *J. Magn. Reson.* **1995**, *A115*, 183.
(4) Prisner, T. F.; Rohrer, M.; Möbius, K. *Appl. Magn. Reson.* **1994**, *7*, 167.
(5) Paschedag, L.; van Tol, J.; Wyder, P. *Rev. Sci. Instrum.* **1995**, *66*, 5098.
(6) Rohrer, M.; Plato, M.; MacMillan, F.; Grishin, Y.; Lubitz, W.; Möbius, K. *J. Magn. Reson.* **1995**, *A 116*, 59.
(7) Coremans, J. W. A.; Poluektov, O. G.; Groenen, E. J. J.; Canters, G. W.; Nar, H.; Messerschmidt, A. *J. Am. Chem. Soc.* **1996**, *118*, 12141.
(8) Goldfarb, D.; Strohmaier, K. G.; Vaughan, D. E. W.; Thomann, H.; Poluektov, O. G.; Schmidt, J. *J. Am. Chem. Soc.* **1996**, *118*, 4665.
(9) Bennebroek, M. T.; Poluektov, O. G.; Zakrzewski, A. J.; Baranov, P. G.; Schmidt, J. *Phys. Rev. Lett.* **1995**, *74*, 442.
(10) Burghaus, O.; Plato, M.; Rohrer, M.; Möbius, K.; MacMillan, F.; Lubitz, W. *J. Phys. Chem.* **1993**, *97*, 7639.
(11) Möbius, K. In *EMR of Paramagnetic Molecules* Berliner, L. J., Reuben, J., Eds.; Plenum: New York, 1993; p 253.
(12) Prisner, T. F.; McDermott, A. E.; Un, S.; Norris, J. R.; Thurnauer, M. C.; Griffin, R. G. *Proc. Natl. Acad. Sci. U.S.A.* **1993**, *90*, 9485.
(13) Isaacson, R. A.; Lendzian, F.; Abresch, E. C.; Lubitz, W.; Feher, G. *Biophys. J.* **1995**, *69*, 311.
(14) Rist, G.; Hyde, J. S. *J. Chem. Phys.* **1968**, *49*, 2449; **1969**, *50*, 4532; **1970**, *52*, 4633.
(15) Greiner, S. P.; Kreilick, R. W. *J. Magn. Reson.* **1992**, *100*, 43.
(16) Hüttermann, J. *Biol. Magn. Reson.* **1993**, *13*, 219.
(17) Hoffman, B. M.; DeRose, V. J.; Doan, P. E.; Gurbiel, R. J.; Houseman, A. L.; Telser, J. *Biol. Magn. Reson.* **1993**, *13*, 151.
(18) Okamura, M. Y.; Debus, R. J.; Kleinfeld, D.; Feher, G. In *Function of Quinones in Energy Conserving Systems*; Trumpower, B. L., Ed., Academic: 1982; p 299.
(19) Okamura, M. Y.; Feher, G. In *Anoxygenic Photosynthetic Bacteria*; Blankenship, R. E., Madigan, M. T., Bauer, C. E., Eds.; Kluwer: Dordrecht, 1995; p 577.
(20) Lancaster, C. R. D.; Ermler, U.; Michel, H. In *Anoxygenic Photosynthetic Bacteria*; Blankenship, R. E., Madigan, M. T., Bauer, C. E., Eds.; Kluwer: Dordrecht, 1995; p 503.
(21) Feher, G.; Isaacson, R. A.; Okamura, M. Y.; Lubitz, W. In *Antennas and Reaction Centers of Photosynthetic Bacteria*; Michel-Beyerle, M. E., Ed.; Springer: Berlin, 1985; p 174.
(22) van den Brink, J. S.; Spoyalov, A. P.; Gast, P.; van Liemt, W. B. S.; Raap, J.; Lugtenburg, J.; Hoff, A. J. *FEBS Lett.* **1994**, *353*, 273.

(23) Isaacson, R. A.; Abresch, E. C.; Lendzian, F.; Boullais, C.; Paddock, M. L.; Mioskowski, C.; Lubitz, W.; Feher, G. In *The Reaction Center of Photosynthetic Bacteria*; Michel-Beyerle, M. E., Ed.; Springer: Berlin, 1996; p 353.

(24) Brudler, R.; deGroot, H. J. M.; van Liemt, W. B. S.; Steggerda, W. F.; Esmeijer, R.; Gast, P.; Hoff, A. J.; Lugtenburg, J.; Gerwert, K. *EMBO J.* **1994**, *13*, 5523.

(25) Breton, J.; Boullais, C.; Burie, J.-R.; Nabedryk, E.; Mioskowski, C. *Biochemistry* **1994**, *33*, 14378.

(26) Debus, R. J.; Feher, G.; Okamura, M. J. *Biochemistry* **1986**, *25*, 2276.

(27) Lubitz, W.; Abresch, E. C.; Debus, R. J.; Isaacson, R. A., Okamura, M. Y. Feher, G. *Biochim. Biophys. Acta* **1985**, *808*, 464.

(28) Lubitz, W.; Isaacson, R. A.; Abresch, E. C.; Feher, G. *Biophys. J. (Abstracts)* **1993**, *64*, A18.

(29) Isaacson, R. A.; Abresch, E.; Feher, G.; Lubitz, W.; Williams, J. C.; Allen, J. P. *Biophys. J. (Abstracts)* **1995**, *68*, A246.

(30) Davies, E. R. *Phys. Lett.* **1974**, *47a*, 1.

(31) Poole Jr., C. P.; Farach, H. A. In *The Theory of Magnetic Resonance*; Wiley: New York, 1972.

(32) MacMillan, F.; Lendzian, F.; Lubitz, W. *Magn. Reson. Chem.* **1995**, *33*, 81.

(33) Butler, W. F.; Calvo, R.; Fredkin, D. R.; Isaacson, R. A.; Feher, G. *Biophys. J.* **1984**, *45*, 947.

(34) Williams, J. C.; Paddock, M. L.; Feher, G.; Allen, J. P. *Biophys. J. (Abstracts)* **1991**, *59*, 142a.

(35) Paddock, M. L., personal communication.

(36) Rohrer, M.; Gast, P.; Möbius, K.; Prisner, T. F. *Chem. Phys. Lett.* **1996**, *259*, 523.

(37) Prisner, T. F.; In *Advances of Magnetic and Optical Resonance*, Vol. 20; Warren, W. S., Ed., Academic: 1997; p 245.

(38) O'Malley, P. J.; Babcock, G. T. *J. Chem. Phys.* **1984**, *80*, 3912.

(39) O'Malley, P. J.; Chandrashekar, T. K.; Babcock, G. T. In *Antennas and Reaction Centers of Photosynthetic Bacteria*; Michel-Beyerle, M. E., Ed.; Springer: Berlin, 1985; p 339.

(40) Pedersen, J. A. *Handbook of EPR Spectra from Quinones and Quinols*; CRC: Boca Raton, FL, 1985.

(41) McConnell, H. M.; Strathdee, J. *Mol. Phys.* **1959**, *2*, 129.

(42) Bosch, M. K.; Gast, P.; Hoff, A. J.; Spoyalov, A. P.; Tsvetkov, Y. D. *Chem. Phys. Lett.* **1995**, *239*, 306.

(43) Lendzian, F,; Rautter, J.; Käss, H.; Gardiner, A.; Lubitz, W. *Ber. Bunsen-Ges. Phys. Chem.* **1996**, *100*, 2036.

(44) Stowell, M. H. B.; McPhillips, T. M.; Rees, D. C.; Soltis, S. M.; Abresch, E.; Feher, G. *Science* **1997**, *276*, 812.

(45) Lubitz, W.; Feher, G. submitted for publication in *Appl. Magn. Reson.*